

Measurement of the $^{241}\text{Am}(n, 2n)$ reaction cross section from 7.6 MeV to 14.5 MeV

A. P. Tonchev,¹ C. T. Angell,² M. Boswell,² A. S. Crowell,¹ B. Fallin,¹ S. Hammond,² C. R. Howell,¹
A. Hutcheson,¹ H. J. Karwowski,² J. H. Kelley,³ R. S. Pedroni,⁴ and W. Tornow¹

¹Duke University and TUNL, Durham, NC 27708, USA

²University of North Carolina at Chapel Hill and TUNL, Chapel Hill, North Carolina 27599, USA

³North Carolina State University and TUNL, Raleigh, North Carolina 27695, USA

⁴North Carolina A&T State University and TUNL, Greensboro, North Carolina 27411, USA

J. A. Becker, D. Dashdorj, J. Kenneally, R. A. Macri,
M. A. Stoyer, and C. Y. Wu

Lawrence Livermore National Laboratory, Livermore, California 94550, USA

E. Bond, M. B. Chadwick, J. Fitzpatrick, T. Kawano, R. S. Rundberg,
A. Slemmons, D. J. Vieira, and J. B. Wilhelmly

Los Alamos National Laboratory, Los Alamos, New Mexico 87545, USA

(Received 5 March 2008; published 27 May 2008)

The $(n, 2n)$ cross section of the radioactive isotope ^{241}Am ($T_{1/2} = 432.6$ y) has been measured in the incident neutron energy range from 7.6 to 14.5 MeV in steps of a few MeV using the activation technique. Monoenergetic neutron beams were produced via the $^2\text{H}(d, n)^3\text{He}$ reaction by bombarding a pressurized deuterium gas cell with an energetic deuteron beam at the TUNL 10-MV Van de Graaff accelerator facility. The induced γ -ray activity of ^{240}Am was measured with high-resolution HPGe detectors. The cross section was determined relative to Al, Ni, and Au neutron activation monitor foils, measured in the same geometry. Good agreement is obtained with previous measurements at around 9 and 14 MeV, whereas for a large discrepancy is observed when our data are compared to those reported by Perdikakis *et al.* near 11 MeV. Very good agreement is found with the END-B/VII evaluation, whereas the JENDL-3.3 evaluation is in fair agreement with our data.

DOI: [10.1103/PhysRevC.77.054610](https://doi.org/10.1103/PhysRevC.77.054610)

PACS number(s): 24.60.Dr, 25.40.Fq, 25.45.-z, 25.60.Dz

I. INTRODUCTION

Accurate neutron-induced reaction cross-section data are required for many practical applications, especially in the field of nuclear energy. The cross sections are needed, for example, to estimate the decay heat, activation of structural materials, and gas production in both present day fission and future fusion reactors. Here we concentrate on fast neutron induced reactions on the minor actinide ^{241}Am . Improved neutron induced measurements on the minor actinides are desired for the Global Nuclear Energy Partnership, the transmutation of long-lived radioactive waste with advanced high neutron-energy reactors [1,2], and establishing improved diagnostics for nuclear device performance.

There exist only a few measurements on the $^{241}\text{Am}(n, 2n)$ reaction. Most of the previous data were obtained at neutron energies around 14 MeV [3–5]. Recent evaluations show a large spread in the predicted cross section for this reaction [6]. Therefore, not surprisingly, the only region where the predicted cross section from JEF-3.0, JENDL-3.3, BROND-2.2, and ENDF/B-VII describe the $(n, 2n)$ data reasonably well is around 14 MeV. However, very recently new data were published at $8 < E_n < 11$ MeV [7]. These data obtained with the activation technique show a steep increase of the $^{241}\text{Am}(n, 2n)$ cross section from 8.8 to 11 MeV, in contrast to most of the theoretical predictions that are almost a factor of 2 lower at 11 MeV. Obviously, the energy region around $E_n = 11$ MeV needs more experimental study. In the

following we report on new data for the excitation function of the $^{241}\text{Am}(n, 2n)$ reaction from near threshold to 14.5 MeV incident neutron energy, and we compare these data with statistical nuclear-model calculations performed with the GNASH code [8].

II. EXPERIMENT

A. Experimental setup for activation measurements

In this work the excitation function for the reaction $^{241}\text{Am}(n, 2n)^{240}\text{Am}$ has been measured from 7.6 to 14.5 MeV using the activation technique. Highly enriched ^{241}Am targets of 99.9% were irradiated with monoenergetic neutrons produced by the $^2\text{H}(d, n)^3\text{He}$ reaction ($Q = 3.269$ MeV) using deuteron beams from the TUNL 10-MV FN Tandem Van de Graaff accelerator. A 2- μA deuteron beam, collimated to rectangular shape with 3 mm, entered through a 6.35- μm -thick Havar foil into a 3-cm-long and 1-cm-diameter deuterium gas cell pressurized to 3 atm. The deuteron beam was stopped in a tungsten beam stop that formed the end of the gas cell. By selecting incident deuteron energies between 5.0 and 11.9 MeV, quasi-monoenergetic neutron beams with energies between 7.6 and 14.5 MeV were produced.

The americium targets were placed in thin aluminum containers sealed with 2-cm-diameter Havar windows. The targets were positioned 3.3 cm from the end of the deuterium

gas cell. The neutron flux was measured by 1-cm-diameter Al, Ni, and Au foils placed in the irradiation containers at 1.5 mm upstream and 1.5 mm downstream of the ^{241}Am targets. The average neutron flux produced at the target position (4.8 cm from the center of the gas cell) depended on the deuteron energy [9] and varied between 1×10^7 to $5 \times 10^7 \text{ cm}^{-2} \text{ s}^{-1}$. Monte Carlo neutron-transport calculations have been performed to determine the neutron energy distribution “seen” by the target assembly. Considering the neutron production kinematics and the gas cell-target geometry, the energy spread of the neutron beam was found to vary between 65 and 145 keV (FWHM), with the smaller energy spread associated to the higher neutron energies.

During each activation period, variations in the neutron flux were measured using three NE-213 liquid scintillator detectors located 4.77 m from the gas cell at angles of 0° (coaxial with the target), -10° , and $+10^\circ$, relative to the incident deuteron beam. Corrections due to the time dependence of the neutron flux, as well as beam on/off corrections were applied to all of the activation products investigated. The irradiation periods ranged from 24 to 72 h, depending on the separation of the incident neutron energy from the reaction threshold. Total neutron fluences of $(1-5) \times 10^{12}$ were produced during these times.

At the end of the activation period the neutron energy calibration (i.e., deuteron energy of the Tandem accelerator and deuterium energy loss in the deuterium gas cell) was verified using the neutron attenuation technique applied to the known resonance in n - ^{12}C scattering at $E_n = 7.745 \text{ MeV}$. The measured neutron energy was found to be in very good agreement ($<30 \text{ keV}$) with the value calculated from the deuteron beam mean energy as determined from the setting of the tandem Van de Graaff beam analyzing magnet and beam energy loss calculations in the gas cell.

B. Radioactive ^{241}Am target preparation

^{241}Am samples were produced at Los Alamos National Laboratory (LANL) as a dry nitrate. After further chemical purification electroplated targets were fabricated at Lawrence Livermore National Laboratory (LLNL). A Dowex 50×4 cation exchange column was used to remove alkalis, some transition metals, and Ca. The sample was then passed down a Dowex 1×8 anion exchange column for further purification. A $12.7\text{-}\mu\text{m}$ -thick Pt foil was used as the target backing material and a 1-cm-diameter layer of ^{241}Am was electroplated from an isopropanol/dilute nitric acid solution in layers by applying an electrical potential between a Pt electrode and the target backing. A thin layer was deposited first ($10 \mu\text{g}/\text{cm}^2$) to prepare the surface for additional layers, and then thicker layers of $100 \mu\text{g}/\text{cm}^2$ were deposited until a total thickness of about $500 \mu\text{g}/\text{cm}^2$ was achieved. After each layer was deposited, the target was heated in a furnace at 500°C for 20 min to convert the Am to its oxide. The target thickness was monitored after each layer deposit both by γ -ray and α -particle counting, which gave consistent results within experimental uncertainties. The target uniformity was monitored visually. Two electroplated targets were then epoxied together and the

TABLE I. ^{241}Am target characteristics.

Target no.	Diameter (mm)	Thickness ($\mu\text{g}/\text{cm}^2$)	Mass (μg)	Total activity ^a (mCi)
1 ^b	10.0	993	780(16)	2.67
2 ^b	10.0	1007	791(16)	2.71
3 ^b	10.0	1141	897(18)	3.07
4 ^b	10.0	1032	811(16)	2.78
5 ^b	10.0	1002	787(16)	2.70
6 ^b	10.0	1024	787(16)	2.76
2 ^c	10.0	1121	1015(20)	3.48
3 ^c	10.0	1168	1100(22)	3.77
4 ^c	10.0	1096	950(19)	3.25

^a $1 \text{ mCi} = 3.7 \times 10^7 \text{ Bq}$.

^b Electroplated target.

^c Stippled target.

assembly was epoxied onto two target rings and sealed with clear spray paint. A drawing of the target is presented in Fig. 1. The total ^{241}Am target thickness was approximately $1 \text{ mg}/\text{cm}^2$. Six electroplated targets of $\sim 1 \text{ mg}/\text{cm}^2 \times 1 \text{ cm}$ diameter were prepared at LLNL. These targets were used to obtain most of the data presented in this article. In addition three stippled ^{241}Am targets of the same dimension were fabricated at LANL from the original material. Table I summarizes the characteristics of the targets produced for our experiments.

C. Activation measurements

After each irradiation the target assembly was dismantled so that the front and back monitor foil stacks could be counted separately from the ^{241}Am target in the same counting geometry. The neutron flux during each irradiation was determined via the three monitor reactions, $^{27}\text{Al}(n, \alpha)^{24}\text{Na}$, $^{58}\text{Ni}(n, p)^{58}\text{Cu}$, and $^{197}\text{Au}(n, 2n)^{196}\text{Au}$. Decay properties of these reactions are given in Table II. The two strongest lines that dominate the decay spectrum of ^{240}Am are also given

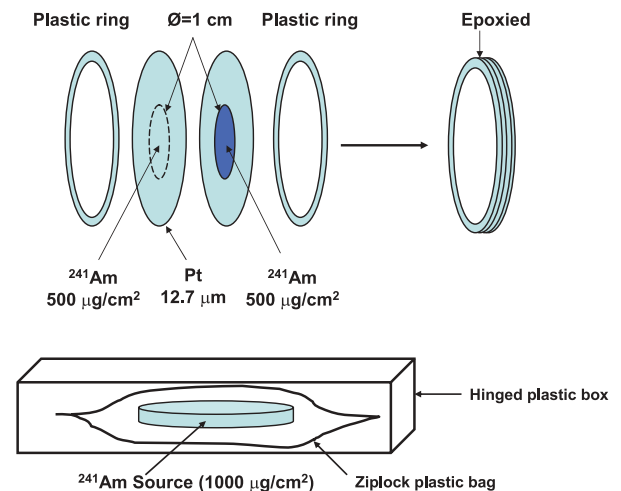


FIG. 1. (Color online) Construction and details of a typical ^{241}Am target.

TABLE II. Decay properties of the monitor reactions used for neutron flux normalization. Only the strongest transitions are given here. Isotopic and decay data characteristics are from Ref. [6].

Reaction	Isotopic abundance (%)	Q value (keV)	Half-life (h)	Decay mode (% branching)	γ -ray energy (keV)	γ -ray intensity (%)
Monitor reactions						
$^{27}\text{Al}(n, \alpha)^{24}\text{Na}$	100.0	-3132.14(0.14)	14.9590(12)	β^- (100)	1368.630(6)	100.0
$^{58}\text{Ni}(n, p)^{58}\text{Co}$	68.077	400.52(1.39)	29525.00(144)	EC ^a (100)	810.76(10)	99.45(1)
$^{197}\text{Au}(n, 2n)^{196}\text{Au}$	100.0	-8072.30(2.94)	148.392(240)	β^- (7.20) EC(92.80)	355.73(5)	87.00(8)
Investigated reaction						
$^{241}\text{Am}(n, 2n)^{240}\text{Am}$	99.9	-6647.1(13.8)	50.8(3)	EC(100.0) α (1.9E-4)	987.76(6) 888.80(5)	72.2(7) ^b 25.1(4) ^b

^aElectron capture.

^bTaken from Ref. [10].

in the bottom part of Table II [6]. The recent evaluation of Browne [10] significantly reduced the uncertainties of these two transitions. The new values for the γ -ray intensities allow us to decrease the overall uncertainties of the $^{241}\text{Am}(n, 2n)$ reaction cross section.

Three 60% HPGe detectors combined with a Canberra Multiport II multichannel analyzer and 16 K ADC, fully supported by the Genie 2000 data-acquisition system, were used to count the residual activity of the americium targets and monitor foils. The sample-to-detector front face distance was 3 cm. The activated americium targets and monitor foils were measured in 1-h intervals for several days to follow their decay activity. To attenuate the strong rate of the 59.5-keV γ rays emitted by the ^{241}Am target, one 3-mm-thick disk of lead was placed directly in front and one 3-mm disk directly behind of each target before counting. This attenuated the intensity of the 59.5-keV γ rays by 10^7 , whereas it reduced the 888.8- and 987.8-keV γ rays associated with the decay of the $(n, 2n)$ reaction product ^{240}Am by 23 and 21%, respectively.

Because the counts in the full energy peak of the γ -ray transitions are used to determine the activity of the samples, the knowledge of the photopeak detection efficiency for the counting geometry is required. For this purpose and for the energy calibration of all detectors, several calibrated single and multi- γ -ray point sources and an extended ^{152}Eu source with an active diameter of 1 cm were used. The extended ^{152}Eu source eliminated the geometry difference between the point sources and the americium target disk. The calibrated sources were positioned in the same counting containers and were sandwiched between the same 3-mm lead absorbers. The bottom panel of Fig. 2 shows the high-energy portion of a γ -ray spectrum collected after irradiating the ^{241}Am target. Spectra from the platinum backing after irradiation (top panel) and the ^{241}Am target before activation (middle panel) are also shown. Many of the peaks observed in the americium spectra are due to weak transitions from the decay of ^{241}Am or from activation of the platinum backing. By tracking the time dependence of the decay of the 888.8-keV level, it was determined that this peak was partially contaminated by a weak unresolved transition from ^{241}Am at 887.3 keV (see central panel of Fig. 2). Hence, the transition at 988 keV was chosen for cross-section analysis, because it was free of contaminations.

III. EXPERIMENTAL RESULTS AND ANALYSIS

For any particular γ -ray transition the number of events S registered in the HPGe detector during the activation are given by the expression

$$S = \frac{N\theta I_{\gamma}\epsilon_{\gamma}}{\lambda} (1 - e^{-\lambda t_i}) e^{-\lambda t_d} (1 - e^{-\lambda t_m}) \left(\prod_k C_k \right) \times \int_{E_{\text{th}}}^{E_{\text{max}}} \Phi(E, E_{\text{max}}) \sigma(E) dE, \quad (1)$$

where S is the observed number of γ rays, $N = \frac{m\theta N_A}{M}$ is the number of target nuclei, m is the target mass, θ is the isotopic abundance, N_A is the Avogadro number, M is the atomic mass,

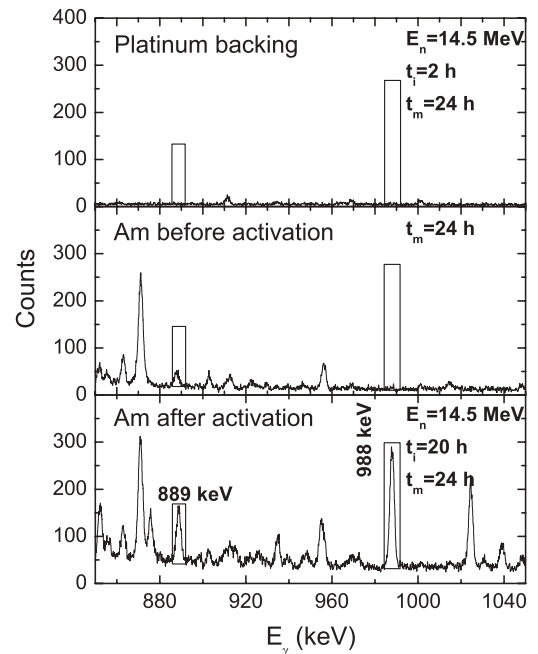


FIG. 2. High-energy portion of γ -ray spectra collected for the platinum backing (top) and the americium target (bottom) after activation with 14.5-MeV neutrons, and the americium target before activation (center). γ -ray lines at 888.8 and 987.8 keV associated with the decay of ^{240}Am are indicated.

I_γ is the γ -ray intensity, ϵ_γ is the detector efficiency, λ is the decay constant, and t_i, t_d, t_m , are the irradiation, decay, and measurement times, respectively. The factor C_k is the correction factor that takes into account breakup neutrons produced in our gas cell, flux fluctuation, and coincidence summing. The quantity $\Phi(E, E_{\max})$ is the neutron energy distribution, and $\sigma(E)$ is the cross section of interest.

If the neutron energy interval is small enough so that the cross section does not change significantly, the integral in [Eq. (1)] can be defined as the product of two Δ functions

$$S = NI_\gamma \epsilon_\gamma f(t) \Delta \Phi \Delta \sigma \prod_k C_k, \quad (2)$$

where $f(t) = (1 - e^{-\lambda t_i})e^{-\lambda t_d}(1 - e^{-\lambda t_m})/\lambda$ is the time factor, $\Delta \Phi$ is the neutron flux, and $\Delta \sigma$ is the average neutron cross section over the neutron energy distribution $\Delta \Phi$.

The activation formula [Eq. (1)] assumes a constant neutron flux during the time of irradiation. Due to fluctuations in the deuteron beam intensity the neutron flux varied during long irradiation times. Corrections to the measured $^{241}\text{Am}(n, 2n)^{240}\text{Am}$ and monitor reaction yields were applied to account properly for the time profile of the neutron flux in the activation formula. The correction factor c_{flux} for flux fluctuations was calculated from the ratio

$$c_{\text{flux}} = \frac{\bar{\Phi}(1 - e^{-\lambda t_i})}{\sum_{i=1}^n \Phi_i(1 - e^{-\lambda \Delta t})e^{-\lambda(n-i)\Delta t}}, \quad (3)$$

where $\bar{\Phi}$ is the mean flux during the irradiation, Φ_i is the flux during the time bin i , n is the number of total time bins, t_i is the irradiation time, and Δt is the dwell time. Because the ^{241}Am cross-section measurements were carried out relative to ^{27}Al , ^{58}Ni , and ^{197}Au as standards, the neutron flux can be determined by measuring γ -ray yields from these reactions (see Sec. II C). For each given mean neutron energy the standard cross-section value was obtained by linear interpolation of the tabulated data given in Ref. [6]. Finally, the americium cross section was calculated from the following activation formula [11]:

$$\sigma^{\text{Am}} = \frac{S^{\text{Am}}}{N^{\text{Am}} I_\gamma^{\text{Am}} \epsilon_\gamma^{\text{Am}} f(t)^{\text{Am}} \Delta \Phi^{\text{st}} \prod_k C_k^{\text{Am}}}. \quad (4)$$

At the end of the activation periods the Tandem accelerator was operated in the pulsed deuteron-beam mode with a repetition rate of 2.5 MHz and neutrons time-of-flight (TOF) spectra at 0° were obtained at $E_n = 8, 10, 12,$ and 14 MeV. The experimental setup is described in more detail in Ref. [9]. The TOF technique permitted us to estimate the contribution of background neutrons in the same experimental conditions as those of the activation measurements. The peak shown in Fig. 3 and centered around channel number 700 is due to the monoenergetic neutrons produced via the $^2\text{H}(d, n)^3\text{He}$ reaction. The broader distribution centered around channel number 500 is from neutrons produced in deuteron breakup reactions in the gas cell. The peak at channel number 900 is the “ γ -flash” resulting from reactions in the beam stop and the Havar foil of the gas cell. The TOF spectra were also used to calculate the whole neutron energy spectrum that is divided into a breakup part and a monoenergetic part. The ratio of the activity induced by monoenergetic neutrons to that induced by

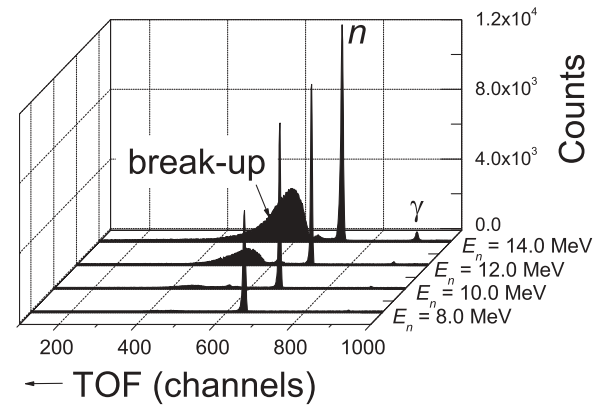


FIG. 3. TOF spectra obtained with 0° neutron monitor at $E_n = 8.0, 10.0, 12.0,$ and 14.0 MeV. The continuum at channel numbers below 600 is due to deuteron-breakup reactions in the gas cell. The symbols n and γ label the neutron and γ -ray peaks, respectively.

breakup neutrons was calculated and used for correcting the cross-section data for contributions of breakup neutrons. The corrections were of the order of a few percentages (except for the Ni monitor foil). They strongly depended on the neutron energy, the reaction threshold and the excitation function of the reactions of interest.

Using the measured 987.8-keV ^{240}Am yields with the calibrated γ -ray efficiency, neutron fluence determinations obtained from the monitor foil yields and ENDF/B-VII monitor reaction cross sections, target thickness assay, on/off beam corrections, and decay scheme information, the $(n, 2n)$ cross section has been calculated for each irradiation. The average neutron flux density at the americium target position was obtained by taking the average value of the neutron flux deduced from the front and the back monitor foil activities. The cross-section data measured in the incident neutron energy range from 7.6 to 14.5 MeV and normalized to the three monitor reactions discussed above are shown in Fig. 4. Labeled

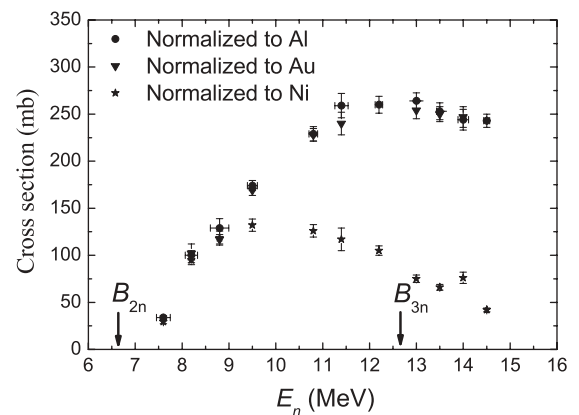


FIG. 4. Excitation function of the $^{241}\text{Am}(n, 2n)^{240}\text{Am}$ reaction normalized to Al, Au, and Ni foils. The horizontal bars indicate the neutron energy spread. The vertical error bars represent the statistical uncertainties of our data. The neutron flux deduced from the Ni monitor foil has not been corrected for breakup-neutron contributions and, therefore, produces incorrect $^{241}\text{Am}(n, 2n)^{240}\text{Am}$ cross-section results.

TABLE III. $^{241}\text{Am}(n, 2n)^{240}\text{Am}$ cross section data.

E_n (MeV)	$^{27}\text{Al}(n, \alpha)$ (mb)	$^{197}\text{Au}(n, 2n)$ (mb)	$^{241}\text{Am}(n, 2n)^{240}\text{Am}^a$ (mb)	$^{241}\text{Am}(n, 2n)^{240}\text{Am}^b$ (mb)	$^{241}\text{Am}(n, 2n)^{240}\text{Am}^c$ (mb)
7.59(15)	29	–	34(2)	–	34(2)
8.18(13)	46	3	100(5)	102(10)	100(5)
8.68(20)	63	120	129(10)	117(5)	120(4)
9.48(11)	82	706	174(5)	169(5)	172(4)
10.78(9)	103	1558	229(8)	228(7)	228(5)
11.30(14)	112	1602	259(13)	240(12)	249(9)
12.17(8)	119	2008	260(9)	–	260(9)
12.97(7)	124	2107	264(9)	254(9)	259(6)
13.46(7)	124	2050	253(9)	250(8)	251(6)
13.91(11)	120	2117	244(11)	247(11)	246(8)
14.46(7)	113	2166	243(7)	–	243(7)

^aNormalized to the $^{27}\text{Al}(n, \alpha)$ reaction.^bNormalized to the $^{197}\text{Au}(n, 2n)$ reaction.^cMean value from (a) and (b).

as B_{2n} and B_{3n} are the threshold energies for the $(n, 2n)$ and $(n, 3n)$ reactions, respectively. The $^{241}\text{Am}(n, 2n)^{240}\text{Am}$ reaction cross-section values are normalized to the neutron flux determined from the Al, Au, and Ni foil data up to $E_n = 9.0$ MeV, and above this energy only the $^{27}\text{Al}(n, \alpha)^{24}\text{Na}$ and $^{197}\text{Au}(n, 2n)^{196}\text{Au}$ reaction data were used. Above $E_n = 9.0$ MeV, corrections for breakup neutrons must be applied to the $^{58}\text{Ni}(n, p)$ reaction data because this reaction is very sensitive to low-energy neutrons due to its positive Q value. As a result, this reaction is difficult to use for normalization purposes at neutron energies above 9.0 MeV (see Fig. 3), and no attempts have been made to extract corrected $^{241}\text{Am}(n, 2n)^{240}\text{Am}$ cross-section values using the $^{58}\text{Ni}(n, p)$ reaction as a monitor. Therefore, our final data include the $^{58}\text{Ni}(n, p)$ normalization data only for neutron energies below 9.0 MeV. Our experimental results show that the $^{241}\text{Am}(n, 2n)^{240}\text{Am}$ cross section peaks at $E_n = 12$ MeV with a maximum values of 260 mb.

Our values for the $^{241}\text{Am}(n, 2n)^{240}\text{Am}$ reaction cross section normalized to Al and Au monitor foils are given in Table III. The first column shows the neutron energy and its spread (FWHM), the second and third columns show the $^{27}\text{Al}(n, \alpha)^{24}\text{Na}$ and $^{197}\text{Au}(n, 2n)^{196}\text{Au}$ reaction cross-sections data [6,12] used to calculate the neutron flux. The fourth and fifth columns show the calculated americium cross sections obtained using the neutron flux determined from the Al and Au monitor-foil data, respectively. The last column shows the mean value of the $^{241}\text{Am}(n, 2n)^{240}\text{Am}$ cross section with only statistical uncertainties quoted.

Table IV summarizes the sources of uncertainties and their estimated magnitudes. The uncertainty in the excitation function of the monitor reactions was assumed to be 3%. In addition, a 3% uncertainty was assigned to our procedure of determining the average neutron flux. The efficiency of the γ -ray detector (incorporating geometry, self-absorption, and pileup) had an uncertainty of about 2–4%. The uncertainty in the decay data was <1%. In addition to these systematic uncertainties, the major uncertainties were due to

counting statistics (2–4%) and corrections to contributions from low-energy neutrons (3%). Because of low count rates the uncertainties in counting statistics and peak-area analysis were relatively large for measurements at low neutron energy. In the higher neutron energy range of 12–14 MeV, those two uncertainties were much lower, and the major source of uncertainty was the correction associated to breakup neutrons. The total uncertainty in each cross-section value was obtained by combining all the individual uncertainties in quadrature, resulting in overall uncertainties in the range of 6 to 8%.

IV. NUCLEAR-MODEL CALCULATIONS

The cross-section calculations shown as the ENDF/B-VII curve in Fig. 5 were performed by means of the GNASH code [8], which uses the Hauser-Feshbach model coupled with a treatment of preequilibrium, direct, and fission reactions.

TABLE IV. Sources of uncertainties and their magnitudes in percentage.

Statistical uncertainties	Am	Monitors
Count rate (statistics and background)	2–4	<1
γ -ray absorption in sample	<1	<0.1
Sample mass	2 ^a	<1
Total relative uncertainties	4.6	1.7
Systematic uncertainties		
Detector efficiency	2–4	2–4
γ -ray emission probability	1	<1
Half-life	<1	<1
Coincidence summing	<2	<1
Low-energy neutrons	3	3
Neutron flux fluctuation	<1	<1
Reference monitor cross section		2–3 ^b
Overall uncertainty	5.7	5.7

^aDeduced from $\alpha + \gamma$ counting.^bTaken from Refs. [6,12].

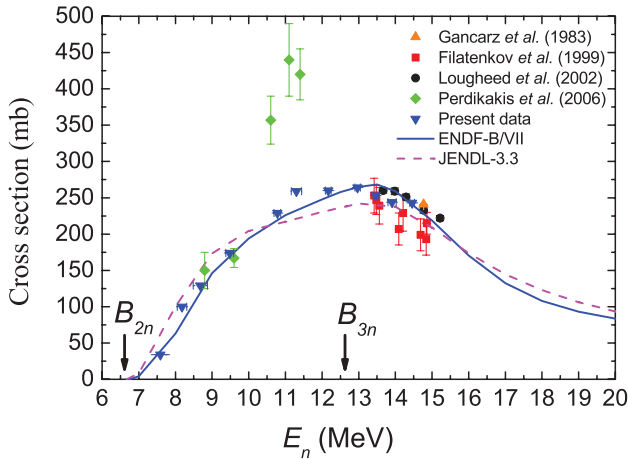


FIG. 5. (Color online) Cross-section measurements for the $^{241}\text{Am}(n, 2n)$ reaction by Gancarz (orange triangles), Filatenkov (red squares), Lougheed (black circles), Perdikakis (green diamonds), and the present TUNL results (blue downward-pointing triangles) compared to JENDL-3.3 (magenta dashed line) and ENDF/B-VII (blue solid line) data evaluations. The ENDF/B-VII evaluation and the underlying GNASH model calculations were published prior to our measurements.

This analysis was performed prior to the measurements reported here, and the calculated predictions and the ENDF/B-VII evaluation were published previously in Refs. [1,13]. Therefore, here we only provide a brief summary of those calculations.

The calculations use a deformed coupled optical potential to represent the neutron scattering on ^{241}Am and to obtain transmission coefficients for the Hauser-Feshbach calculations. This potential was developed to model the measured neutron total and scattering data on americium. The pre-equilibrium reactions were calculated with the exciton model, with input parameters (e.g., the damping matrix element) taken from our systematics for such processes in the actinide region, which are expected to vary slowly from actinide isotope to isotope. Fission barriers were obtained through adjustments so as to match the measured $^{241}\text{Am}(n, f)$ data, typically being about 6 MeV for the inner barriers and 0.5–1.2 MeV lower for the outer barriers. Although these barriers were adjusted to best match the fission data, they are in reasonable agreement with the theoretical predictions from Möller’s calculations using his macroscopic-microscopic global nuclear structure model [14]. The barriers are uncertain to about 0.6 MeV.

Because the $(n, 2n)$ cross section is relatively small compared to the larger multichance fission cross section, the uncertainties in the calculated fission and inelastic scattering, together with the uncertainty in the optical-model reaction cross section (at least 5%), result in significant uncertainties in the predicted $(n, 2n)$ cross section. Indeed, initially, before the older 14 MeV $(n, 2n)$ measurements of Lougheed *et al.* [5] and Gancarz *et al.* [3] were made available to us, the calculated predictions for this cross section were poor. For example, the old ENDF/B-VI evaluation was discrepant with the best measurements by $\sim 50\%$. Once we obtained these reliable Lougheed and Gancarz measurements at 14 MeV, we were

able to make small adjustments to some of the input modeling parameters—especially fission barrier and residual nucleus level densities—to match the measurements at 14 MeV. After that, our prediction of the complete $(n, 2n)$ excitation function over all incident neutron energies was more reliable and was the basis of our ENDF/B-VII evaluation. We also performed an uncertainty quantification analysis of our $(n, 2n)$ prediction over this whole range by propagating reasonable uncertainties in the input model parameters and combining uncertainties from the corresponding $(n, 2n)$ predictions with the measured and assessed uncertainties near 14 MeV.

It is evident from Fig. 5 that the predictions for ENDF/B-VII, after calibration to the 14-MeV data, are now validated by our new TUNL measurements.

V. SUMMARY AND OUTLOOK

A detailed measurement of the $^{241}\text{Am}(n, 2n)^{240}\text{Am}$ cross section has been performed from 7.6 to 14.5 MeV using the monoenergetic neutron beams at TUNL. The cross-section values were determined by means of the activation technique using different sets of monitor reactions. Nuclear-model calculations using the GNASH code were performed taking into account the new fission barrier information of ^{241}Am , which was important for the determination of the $(n, 2n)$ reaction cross section. Our experimental results show that the $^{241}\text{Am}(n, 2n)^{240}\text{Am}$ cross section peaks at $E_n = 12$ MeV with a maximum value of 260 ± 9 mb.

The TUNL results are compared with previous measurements reported by Gancarz [3], Filatenkov *et al.* [4], and Lougheed *et al.* [5] near 14 MeV and the recent data by Perdikakis *et al.* at lower energies [7]. The data agree within the reported errors in the 14-MeV energy region. At lower neutron energies the TUNL data disagree with the three data points reported by Perdikakis *et al.* in the 11-MeV region but agree with their findings at 8.8 and 9.6 MeV. The TUNL measurements are supported very well by the ENDF/B-VI data evaluation, whereas the JENDL-3.3 data evaluation provides a fair description of our data.

Finally, the $(n, 2n)$ cross-section measurements will be extended to the radioactive target ^{243}Am ($T_{1/2} = 7370$ y). Our future plans also include photodisintegration of ^{241}Am using the monoenergetic γ -ray beams from the HI γ S facility. The photodisintegration data combined with the neutron induced measurements at TUNL will be an excellent benchmark for testing pre-equilibrium processes in statistical models.

ACKNOWLEDGMENTS

We acknowledge valuable discussions with A. Plompen of Geel regarding uncertainty estimates for the present $(n, 2n)$ data. This work was supported by the National Nuclear Security Administration under the Stewardship Science Academic Alliances Program through Department of Energy grant DE-FG52-06NA26155.

- [1] P. Talou, T. Kawano, P. G. Young, M. B. Chadwick, and R. E. MacFarlane, Nucl. Sci. Eng. **155**, 84 (2007).
- [2] D. J. Vieira, M. Jandel, T. A. Bredeweg *et al.*, International Conference on Nuclear Data for Science and Technology 2007, to be published.
- [3] A. Gancarz *et al.*, 1983, private communication with M. MacInnes, based on 1983 experiment by Gancarz.
- [4] A. A. Filatenkov and S. V. Chuvaev, Phys. At. Nucl. **63**, 1504 (2000).
- [5] R. W. Lougheed, W. Webster, M. N. Namboodiri, D. R. Nethaway, K. J. Moody, L. H. Landrum, R. W. Hoff, R. J. Dupzyk, J. H. McQuaid, R. Gunnink, and E. D. Watkins, Radiochimica Acta **90**, 833 (2002).
- [6] NNDC Online Data Service, ENDF database, <http://www.nndc.bnl.gov/exfor7/endf00.htm> (2007).
- [7] G. Perdikakis, C. T. Papadopoulos, R. Vlastou, A. Lagoyannis, A. Spyrou, M. Kokkoris, S. Galanopoulos, N. Patronis, D. Karamanis, Ch. Zarkadas, G. Kalyva, and S. Kossionides, Phys. Rev. C **73**, 067601 (2006).
- [8] P. G. Young, E. D. Arthur, and M. B. Chadwick, Los Alamos National Laboratory Report No. LA-12343-MS, 1992.
- [9] A. Hutcheson, C. T. Angell, J. A. Becker, M. Boswell, A. S. Crowell, D. Dashdorj, B. Fallin, N. Fotiades, C. R. Howell, H. J. Karwowski, J. H. Kelley, M. Kiser, R. A. Macri, R. O. Nelson, R. S. Pedroni, A. P. Tonchev, W. Tornow, D. J. Vieira, G. J. Weisel, and J. B. Wilhelmy, Nucl. Instrum. Methods B **261**, 369 (2007).
- [10] B. Singh and E. Browne, submitted for inclusion in the Evaluated Nuclear Structure Data File (ENSDF) and publication in Nuclear Data Sheets, March 2008.
- [11] A. P. Tonchev, Yu. P. Gangrsky, A. G. Belov, and V. E. Zhuchko, Phys. Rev. C **58**, 2851 (1998).
- [12] H. Conde, ed., *Nuclear Data Standards for Nuclear Measurements* (NEA Nuclear Data Committee, Paris, 1992).
- [13] M. B. Chadwick, P. Obložinský, M. Herman *et al.*, Nucl. Data Sheets **107**, 2931 (2006).
- [14] P. Möller, J. R. Nix, W. D. Myers, and W. J. Swiatecki, At. Data Nucl. Data Tables **59**, 185 (1995).